This manuscript was accepted by Appl. Phys. Lett. Click here to see the version of record.

Modifications of plasma density profile and thrust by neutral injection in a helicon plasma thruster

Kazunori Takahashi[1],* Yoshinori Takao[2], and Akira Ando[1]

[1]*Department of Electrical Engineering, Tohoku University, Sendai 980-8579, Japan*

[2]*Division of Systems Research, Yokohama National University, Yokohama 240-8501, Japan*

(Dated: October 23, 2016)

Abstract

Argon propellant is introduced from the upstream and downstream sides of a high power helicon plasma thruster. The plasma density profile and the imparted thrust are measured for various upstream and downstream argon flow rates, where the total gas flow rate of 70 sccm and the resultant vacuum chamber pressure of 0.2 mTorr is maintained. It is observed that the imparted thrust increases with an increase in the downstream gas flow rate; simultaneously an upstream-peaking profile of the plasma density observed for the upstream gas injection becomes uniform for the downstream gas injection. The difference in the thrust between the upstream and downstream gas injections is enhanced by increasing the rf power. The observed density profiles are qualitatively consistent with theoretical predictions taking a neutral depletion effect into account.

* kazunori@ecei.tohoku.ac.jp

This manuscript was accepted by Appl. Phys. Lett. Click here to see the version of record.

A plasma momentum is a fundamental physical quantity relating to static and dynamic plasma behaviors in space and astrophysical plasmas [1, 2], and characteristics of artificial plasma devices in laboratories such as plasma reactors for material processing [3] and electric propulsion devices for space propulsion [4]. In steady-state plasmas, force components imparted to the plasma fluid are balanced according to the momentum equation [5]; hence the plasma momentum is mutually associated with the steady-state profiles of the plasma density and potential even for a constant electron temperature. In the electric propulsion devices, the plasma momentum emitted from the system corresponds to a thrust according to the momentum conservation law [6]. Hence the steady-state profiles of the plasma density and potential are expected to affect the momentum ejection, which dominates the propulsion performance, due to momentum gain/loss processes in the non-uniform plasmas.

A helicon plasma thruster consisting of a high-density helicon source and a magnetic nozzle is one of the propulsion concepts being studied vigorously in recent years [7–14]. The previous studies have shown that the thrust is given by force components due to geometrical boundaries and a magnetic expansion yielding an electron diamagnetic acceleration [15–18]; these force components are affected by spatial profiles of the plasma density and temperature as seen in the models. When the high density plasma is produced by the helicon source, a number of laboratory experiments have shown that the neutral depletion induces non-uniform profiles of the neutral density [19–22]. In typical helicon thrusters, the propellant gas is introduced from the upstream side of the cylindrical insulator source tube and ionized by an antenna powered from an rf generator. An analytical model has predicted that an axially asymmetric profile having a maximum plasma density in the upstream side is formed along the axis due to the neutral depletion when introducing the gas from the one end of the source tube, the other end of which has an open boundary for the plasma ejection [23]. It has been considered that the axially asymmetric non-uniformity of the plasma density is caused by the non-uniform profiles of the neutral density and the resultant ionization rate. A numerical analysis in two dimensions [24] and an experiment [25] have also shown the similar density profiles along the axis. When the axially asymmetric density profile having the upstream peak is formed, a non-negligible axial momentum is transferred to the radial wall by the ions lost to the radial wall [26], where an axial electric field arising from a neutral-depletion-induced asymmetric profile of the plasma density is considered to give the axial momentum to the ions via the electrostatic axial acceleration. This interpretation

has also been validated by a two-dimensional particle-in-cell simulation more recently [27]. Therefore, control of the neutral density profile and the resultant profile of the plasma density are important issues affecting the momentum ejection from the system, i.e., the thrust.

Here the propellant gas is introduced from both the upstream and downstream side of the high power helicon thruster, where both the upstream and downstream gas flow rates are individually controlled for the constant total flow rate of the propellant and the vacuum chamber pressure. It is experimentally demonstrated that the neutral-depletion-induced asymmetric profile of the plasma density, which has the upstream peak and causes the momentum and plasma losses to the radial source wall, is inhibited by introducing the gas from the downstream side. Since the modification of the plasma density by the gas injection is consistent with the previous model [23] taking the neutral depletion effect into account, the change of the plasma density profile seems to be due to that of the neutral density profile. The present experiment demonstrates that the thrust increases when the density peak at the upstream side of the source is inhibited.

Figure 1(a) shows the schematic of the experimental setup of the helicon plasma thruster, which is very similar to the previous experiment [25]. Briefly, the helicon plasma thruster consists of a 6.5-cm-diameter and 20-cm-long pyrex glass tube wound by a double-turn rf loop antenna located at $z = -10.5 \pm 1$ cm [28] and a solenoid centered at $z = -3.5$ cm, where $z = 0$ is defined as the downstream edge of the solenoid. The upstream side of the source tube is terminated by an insulator plate at $z = -16$ cm, which has a small center hole for the gas injection. A 1-mm-diameter ceramic tube is inserted into the source via the small hole for the upstream gas injection. A 1-mm-inner diameter ceramic tube connected to another gas feedthrough is also inserted from the downstream open source exit for the downstream gas injection. Both the upstream and downstream gas injection tubes are connected to two different mass flow controllers, respectively. The flow rates introduced from the upstream and downstream sides are labeled as C_{Arup} and C_{Ardown}, respectively; the total mass flow rate is maintained at $C_{Arup} + C_{Ardown} = 70$ sccm ($\simeq 2.1$ mg/s). Three turbomolecular pumping systems are attached to the chamber (one is same as the previous experiment [25] and two of them are added recently); then the pressure measured by an ionization gauge connected to the chamber sideport is about 0.2 mTorr. A dc current I_B is supplied to the solenoid via a vacuum feedthrough and $I_B = 10$ A is chosen in the present experiment. The calculated magnetic field strength on axis is shown in Fig. 1(b). The rf antenna is water-cooled and

powered from a 13.56 MHz rf generator via an impedance matching circuit and a water-cooled vacuum feedthrough, where the rf power can be increased up to $P_{rf} \sim 5$ kW and the error of the rf output power is about 2 %.

Whole the thruster structure is attached to a pendulum thrust balance described previously [29]. A pendulum displacement induced by the plasma production and a calibration coefficient give the force exerted on the thruster including the mechanical and magnetic structures, where this force corresponds to the thrust and the plasma momentum ejected from the system. A 3-mm-diameter planar Langmuir probe (LP) facing radially is mounted on an axially movable motor stage immersed in the chamber. The LP is biased at -90 V and the steady-state ion saturation current I_{is}, which is proportional to the plasma density for the constant electron temperature, is measured. The rf antenna current is also monitored by a Rogowski coil located inside the matching box to estimate the rf power transfer efficiency given by $\eta_p = P_{abs}/P_{rf} = R_p/(R_p + R_{ant})$, where P_{abs}, R_p, and R_{ant} are a power absorbed into the plasma, a plasma resistance, and an antenna resistance, respectively.

The measured thrust is plotted by open squares in Fig. 2 as a function of the gas flow rates (C_{Arup}, C_{Ardown}) from the upstream and downstream sides for $P_{rf} = 5$ kW. The measurement clearly shows that the thrust increases with the increase in C_{Ardown} (the decrease in C_{Arup}). The rf power transfer efficiency η_p is also plotted by crosses in Fig. 2, and η_p slightly decreases from 0.82 to 0.79 when changing the gas flow rates from $(C_{Arup}, C_{Ardown}) = (70,\ 0)$ to (0, 70) sccm. However, the variation of the absorbed power is comparable to the error of the rf output power from the generator, and hence it can be regarded as constant. Therefore, the present experiment demonstrates that the thrust-to-power ratio can be increased by injecting the gas from the downstream side for the constant absorbed rf power. Filled circles in Fig. 2 show the ion saturation current I_{is} of the LP located at $z = 10$ cm and will be mentioned later.

To further characterize the increase in the thrust for the downstream gas injection, the thrust is measured as a function of the rf power P_{rf} for both the cases of (C_{Arup}, C_{Ardown})= (70, 0) and (0, 70) sccm, as plotted by the open circles and squares in Fig. 3(a), respectively. Fitted curves given by aP_{rf}^b are also drawn in Fig. 3(a), where $(a,\ b)$ are fitting coefficients. Needless to say, the thrust increases with the increase in the rf power for both the cases. The ratio of the thrust for the downstream gas injection (T_{down}) to that for the upstream one (T_{up}) is calculated from the fitted curves in Fig. 3(a) and shown in Fig. 3(b). The ratio

This manuscript was accepted by Appl. Phys. Lett. Click here to see the version of record.

is found to increase from about 1.25 for $P_{rf} \sim 1$ kW to 1.42 for $P_{rf} \sim 5$ kW. Therefore the increase in the thrust by the downstream gas injection (or the decrease by the upstream gas injection) is found to be enhanced by increasing the rf power.

The detailed axial measurement of I_{is} is carried out as a function of the flow rates (C_{Arup}, C_{Ardown}) for $P_{rf} = 5$ kW. The linear and semi-logarithm plots of the measured I_{is} on axis are shown in Figs. 4(a) and 4(b), respectively, where the solid lines are added as visual guides. The results in Fig. 4(a) show that the profile has the maximum density in the upstream side of the source tube and the strong density decay is formed along the axis when introducing the propellant gas from the upstream side, as in the previous model [23] and experiment [25]. On the other hand, the density profile is found to get uniform when decreasing C_{Arup} and increasing C_{Ardown}.

The change of the plasma density profile is considered to be due to the neutral density profiles under the high density plasma production as discussed below. Axial profiles of the plasma density for the cases of zero net gas flow rate and a finite net gas flow rate from only the upstream side have been previously analyzed in the one-dimensional model [23]. The downstream side of the source is assumed to be an open boundary for the latter case in the model; this assumption is similar to the case of (C_{Arup}, C_{Ardown})=(70, 0) sccm and the observed density profile having the upstream peak is consistent with the model (see Fig. 3 in Ref. [23]). Here it is considered that the non-uniformity having the high/low neutral densities in the upstream/downstream region is enhanced by the high rf power and the resultant neutral depletion. For the case of the downstream gas injection in the experiment, on the other hand, a part of the neutrals introduced from the downstream side are expected to be bounced at the back wall and supplied to the source region again. In this sense, the experimental situation of the downstream gas injection is somewhat close to the model for the zero net gas flow rate (see Fig. 2 in Ref. [23]). Hence the uniform plasma density profile within the source ($z < 0$) for the downstream gas injection is qualitatively consistent with the theoretical prediction incorporating the neutral depletion effect, where the axial profile of the neutral density is symmetric along the axis even if the neutral depletion occurs; hence the plasma density profile is likewise symmetric. Therefore it is considered that the difference in the thrust and the plasma density profile between the two cases is enhanced by the high rf power, which induces the neutral depletion.

As seen in Fig. 4(b), the ion current I_{is}, i.e., the density in the magnetic nozzle region

($z > 0$), increases with the increase in C_{Ardown} in spite of the similar density at the nozzle entrance ($z = 0$). The ion current I_{is} measured at $z = 10$ cm is plotted by the filled circles in Fig. 2 as a function of (C_{Arup}, C_{Ardown}) and shows the variation similar to the measured thrust. This result implies that the increase in the plasma density within the magnetic nozzle for the downstream gas injection partially contributes to the increase in the thrust, since the thrust component arising from the magnetic nozzle is dominated by the electron diamagnetic drift current proportional to the electron pressure according to the previous study [16]. Although the physical mechanisms of the downstream density variation in Figs. 2 and 4(b) are still unclear, one of the possible reasons is that the two-dimensional structure near the source exit affects the plasma flow dynamics in the magnetic nozzle. A few experiments have shown the two-dimensional structures near the magnetic nozzle [30, 32–35]; it should be mentioned that one of them has shown the modification of the ion orbit by the two-dimensional potential structure [32, 33]. Hence the detailed two-dimensional measurements will be required for this issue. Another possible reason would be the additional ionization in the magnetic nozzle, although the mean-free path of the electron impact ionization for 0.2 mTorr is much longer than the system length. More addressing the thrust generation, the force exerted to the axial back plate is given by the maximum electron pressure [29]. Therefore the force to the back wall is considered to be enhanced for the upstream gas injection due to the presence of the upstream high density plasma as in Fig. 4(a), while the presence of the upstream density peak seems to enhance the loss of the axial momentum to the radial source boundary as demonstrated previously [26]. The individual measurements of these thrust components and the particle-in-cell simulation for the various gas injection configurations will be useful for further understanding of the thrust generation and improvement of the performance.

In summary, the helicon plasma thruster is operated with the propellant gas injection from the upstream and downstream sides, where both the gas flow rates are individually controlled while maintaining the total gas flow rate, the chamber pressure, and the rf power transfer efficiency. The axial plasma density profile inside the source has the maximum at the upstream side for the upstream gas injection, while it is fairly uniform for the downstream gas injection. These results are consistent with the theoretical prediction including the neutral depletion effects. It is clearly demonstrated that the large thrust is obtained for the uniform density profile with the downstream gas injection, compared with the case of the upstream-

making density profile with the upstream gas injection. In other words, the decrease in the thrust-to-power ratio due to the neutral-depletion-induced asymmetric density profile is shown to be inhibited by modifying the gas injection.

The authors would like to thank Prof. Amnon Fruchtman of Holon Institute of Technology for fruitful discussion on the plasma-gas interaction. This work is partially supported by grant-in-aid for scientific research (Grants No. B 16H04084, and A 26247096) from the Japan Society for the Promotion of Science, the Yazaki Memorial Foundation for Science and Technology.

[1] R. E. Ergun, C. W. Carlson, J. P. McFadden, F. S. Mozer, L. Muschietti, and I. Roth, Phys. Rev. Lett. **81**, 826 (1998).

[2] D. L. Meier, S. Koide, and Y. Uchida, Science **291**, 84 (2001).

[3] P.L.G. Ventzek, R.J. Hoekstra, and M.J. Kushner, J. Vac. Sci. Technol. B **12**, 461 (1994).

[4] A. Fruchtman, Phys. Rev. Lett., **96**, 065002 (2006).

[5] M.A. Lieberman and A.J. Lichtenberg, *Principles of Plasma Discharges and Materials Processing*, 2nd ed., Chap. 2 (Wiley, New Jersey, 2005).

[6] D.M. Goebel and I. Katz, *Fundamentals of Electric Propulsion: Ion and Hall Thrusters*, Chap. 2 (Wiley, New Jersey, 2008).

[7] C. Charles, J. Phys. D: Appl. Phys. **42**, 163001 (2009).

[8] S. Pottinger, V. Lappas, C. Charles, and R. Boswell, J. Phys. D: Appl. Phys. **44**, 235201 (2011).

[9] A. Shabshelowitz and A.D. Gallimore, J. Propul. Power **29**, 919 (2013).

[10] L.T. Williams and M.L. Walker, J. Propul. Power **29**, 520 (2013).

[11] T. Harle, S.J. Pottinger, and V.J. Lappas, Plasma Sources Sci. Technol. **22**, 05015 (2013).

[12] S. Shinohara, H. Nishida, T. Tanikawa, T. Hada, I. Funaki, and K.P. Shamrai, IEEE Trans. Plasma Sci. **42**, 1245 (2014).

[13] F.F. Chen, IEEE Trans. Plasma Sci. **43**, 195 (2015).

[14] K. Takahashi, A. Komuro, and A. Ando, Plasma Sources Sci. Technol. **24**, 055004 (2015).

[15] E. Ahedo and M. Merino, Phys. Plasmas **17**, 073501 (2010).

[16] K. Takahashi, T. Lafleur, C. Charles, P. Alexander, and R.W. Boswell, Phys. Rev. Lett. **107**,

235001 (2011).

[17] A. Fruchtman, K. Takahashi, C. Charles, and R.W. Boswell, Phys. Plasmas **19**, 033507 (2012).

[18] K. Takahashi, C. Charles, and R.W. Boswell, Phys. Rev. Lett. **110**, 195003 (2013).

[19] A.W. Degeling, T.E. Sheridan, and R.W. Boswell, Phys. Plasmas **6**, 3664 (1999).

[20] A. Aanesland, L. Liard, G. Leray, J. Jolly, and P. Chabert, Appl. Phys. Lett. **91**, 121502 (2007).

[21] A.M. Keesee and E.E. Scime, Plasma Sources Sci. Technol. **16**, 742 (2007).

[22] C.M. Denning, M. Wiebold and J.E. Scharer, Phys. Plasmas **15**, 072115 (2008).

[23] A. Fruchtman, IEEE Trans. Plasma Sci. **36**, 403 (2008).

[24] E. Ahedo and J. Navarro-Cavallé, Phys. Plasmas **20**, 043512 (2013).

[25] K. Takahashi, Y. Takao, and A. Ando, Appl. Phys. Lett. **108**, 074103 (2016).

[26] K. Takahashi, A. Chiba, A. Komuro, and A. Ando, Phys. Rev. Lett. **114**, 195001 (2015).

[27] Y. Takao and K. Takahashi, Phys. Plasmas **22**, 113509 (2015).

[28] K. Takahashi, Rev. Sci. Instrum. **83**, 083508 (2012).

[29] K. Takahashi, T. Lafleur, C. Charles, P. Alexander, R.W. Boswell, M. Perren, R. Laine, S. Pottinger, V. Lappas, T. Harle, and D. Lamprou, Appl. Phys. Lett. **98**, 141503 (2011).

[30] W. Cox, C. Charles, R.W. Boswell, and R. Hawkins, Appl. Phys. Lett. **93**, 071505 (2008).

[31] C. Charles, R.W. Boswell, and R. Hawkins, Phys. Rev. Lett. **103**, 095001 (2009).

[32] K. Takahashi and T. Fujiwara, Appl. Phys. Lett. **94**, 061502 (2009).

[33] K. Takahashi, Y. Igarashi, and T. Fujiwara, Appl. Phys. Lett. **97**, 041501 (2010).

[34] S.K. Saha, S. Raychaudhuri, S. Chowdhury, M.S. Janaki, and A.K. Hui, Phys. Plasmas **19**, 092502 (2012).

[35] S.K. Saha, S. Chowdhury, M.S. Janaki, A. Ghosh, A.K. Hui, and S. Raychaudhuri, Phys. Plasmas **21**, 043502 (2014).

This manuscript was accepted by Appl. Phys. Lett. Click here to see the version of record.

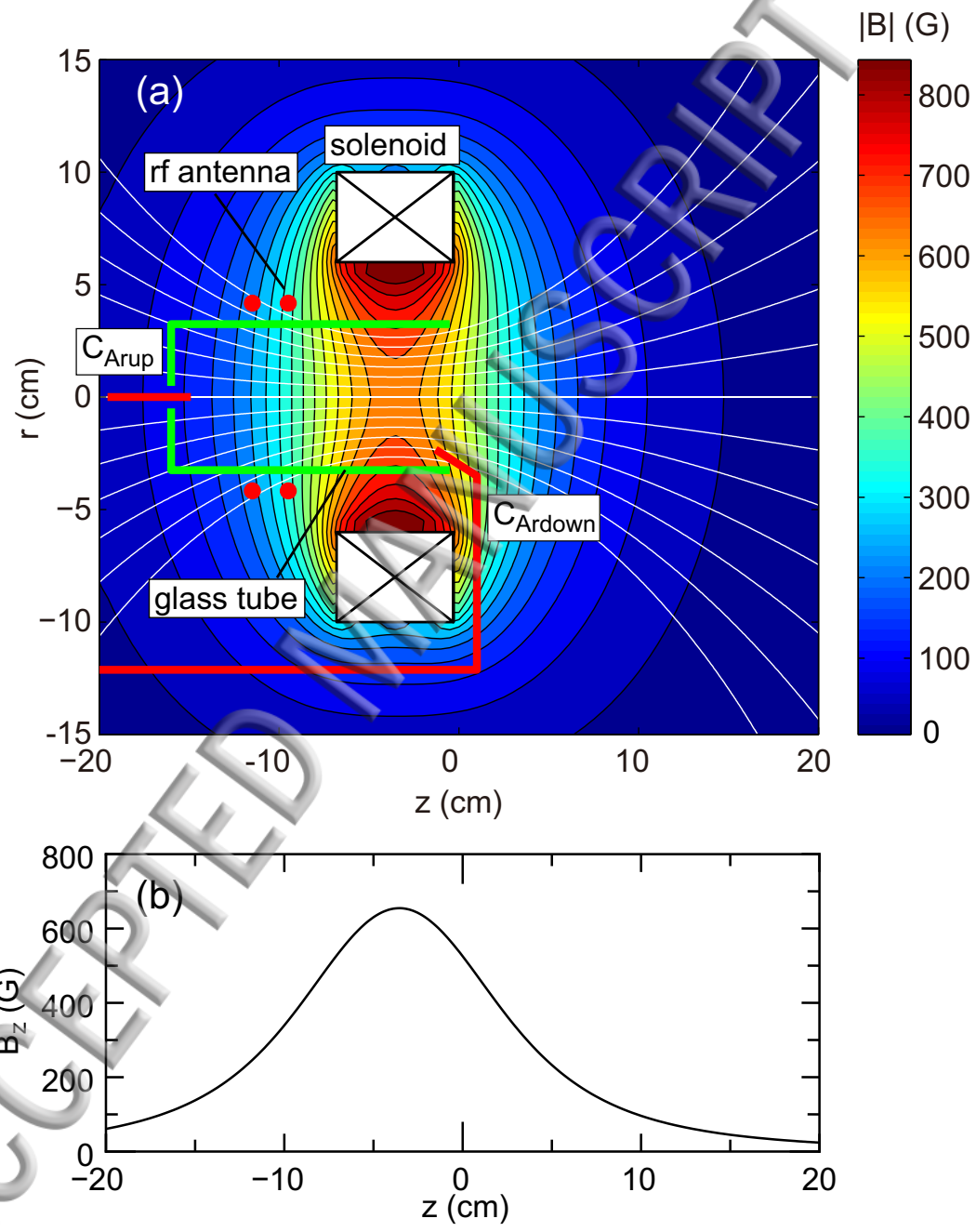

FIG. 1. (a)Schematic of the experimental setup of the helicon thruster immersed in vacuum. The magnetic field strength and lines are shown by the contour color and the solid lines, respectively. (b)Axial profile of the magnetic field strength B_z on axis.

This manuscript was accepted by Appl. Phys. Lett. Click here to see the version of record.

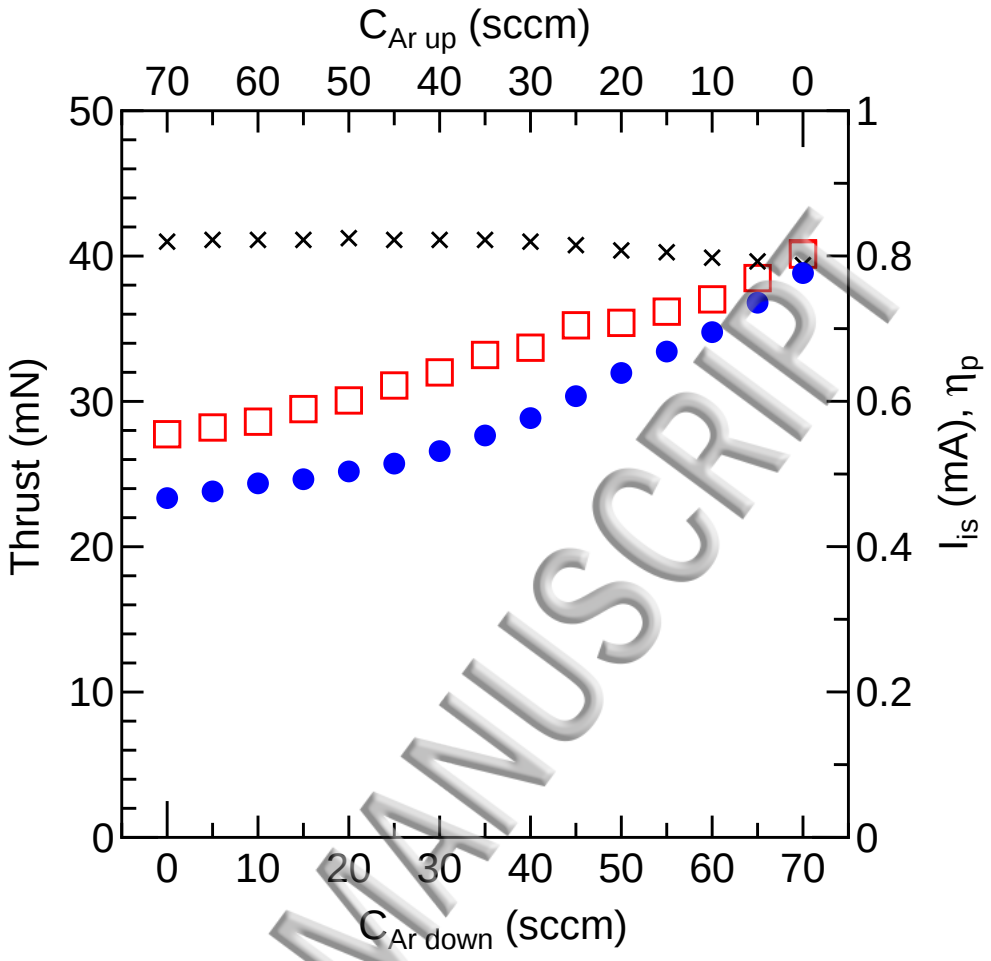

FIG. 2. The measured thrust (open squares), the rf power transfer efficiency η_p (crosses), and the ion saturation current I_{is} (filled circles) of the LP at $z = 10$ cm, as functions of the upstream (C_{Arup}) and downstream (C_{Ardown}) gas flow rates, where the top and bottom axes corresponds to C_{Arup} and C_{Ardown}, respectively.

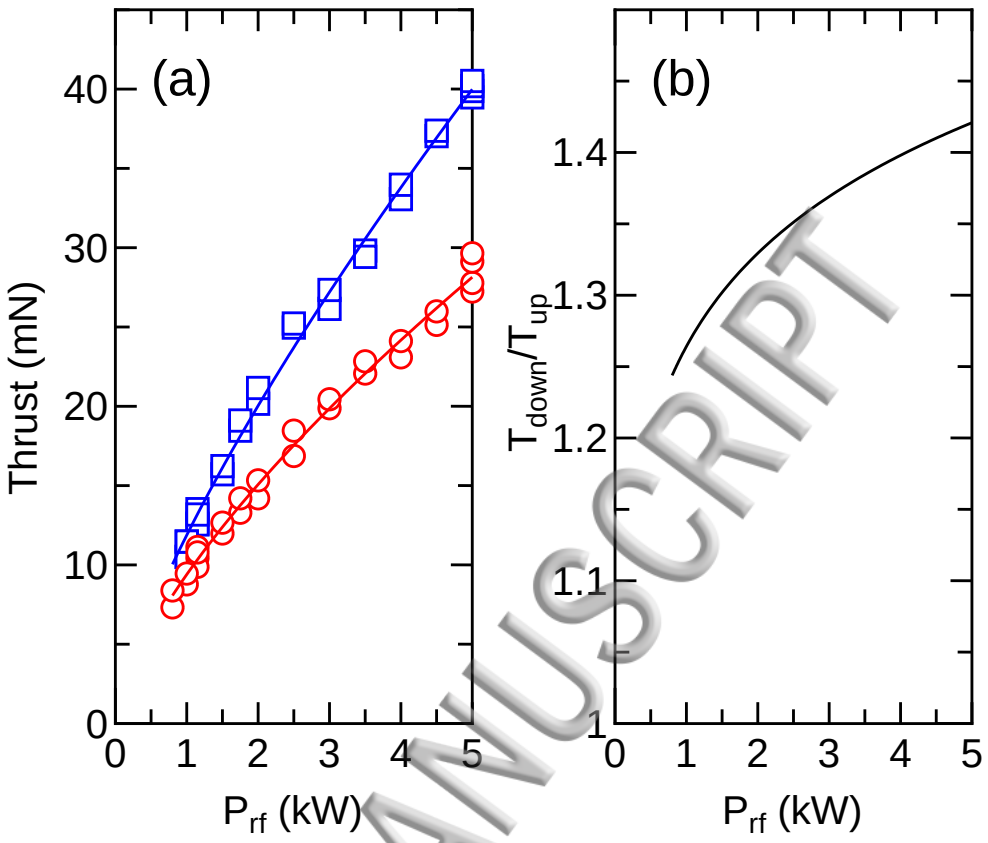

FIG. 3. (a) The measured thrusts as functions of the rf power P_{rf} for (C_{Arup}, C_{Ardown}) = (70, 0) sccm (open circles, defined as T_{up}) and (0, 70) sccm (open squares, defined as T_{down}), together with their fitted curves given by aP_{rf}^{b} with fitting coefficients a and b. (b) Thrust ratio T_{down}/T_{up} calculated from the fitted curves in Fig. 3(a).

This manuscript was accepted by Appl. Phys. Lett. Click here to see the version of record.

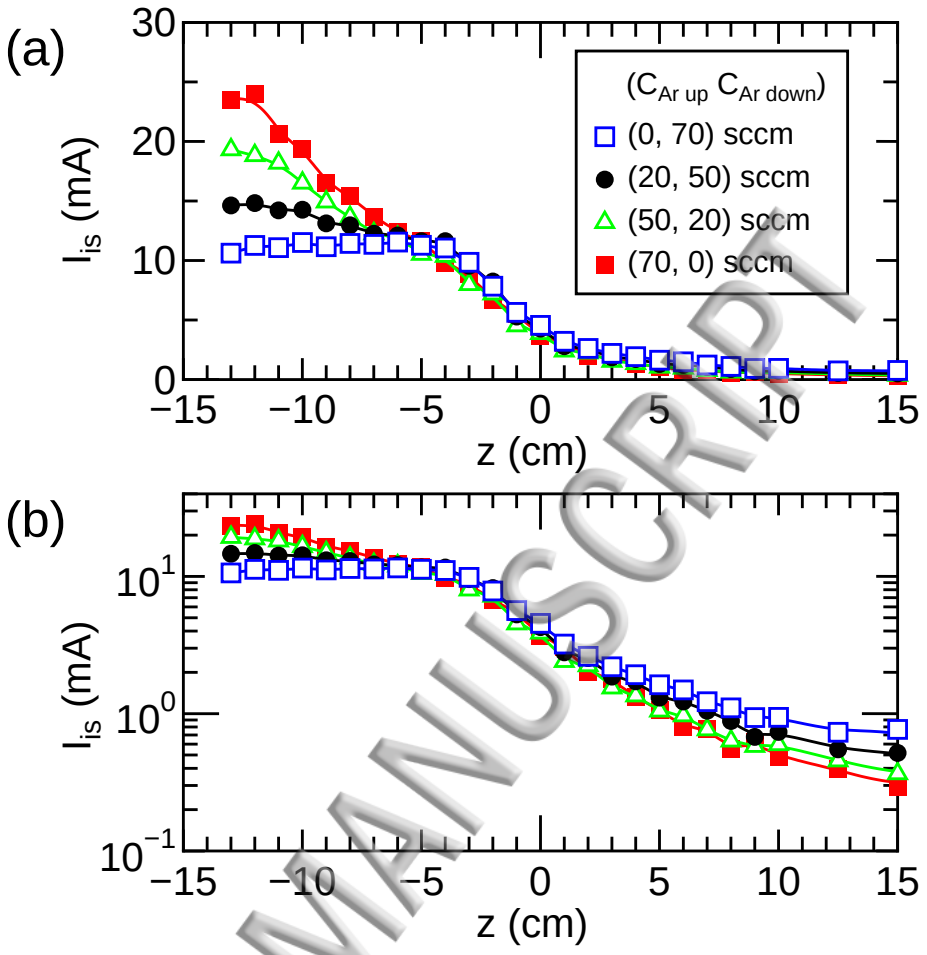

FIG. 4. Axial profile of the ion saturation current I_{is} of the LP on axis as a function of the gas flow rates (C_{Arup}, C_{Ardown}) in the (a) linear and (b) semi-logarithm plots.

This manuscript was accepted by Appl. Phys. Lett. Click here to see the version of record.

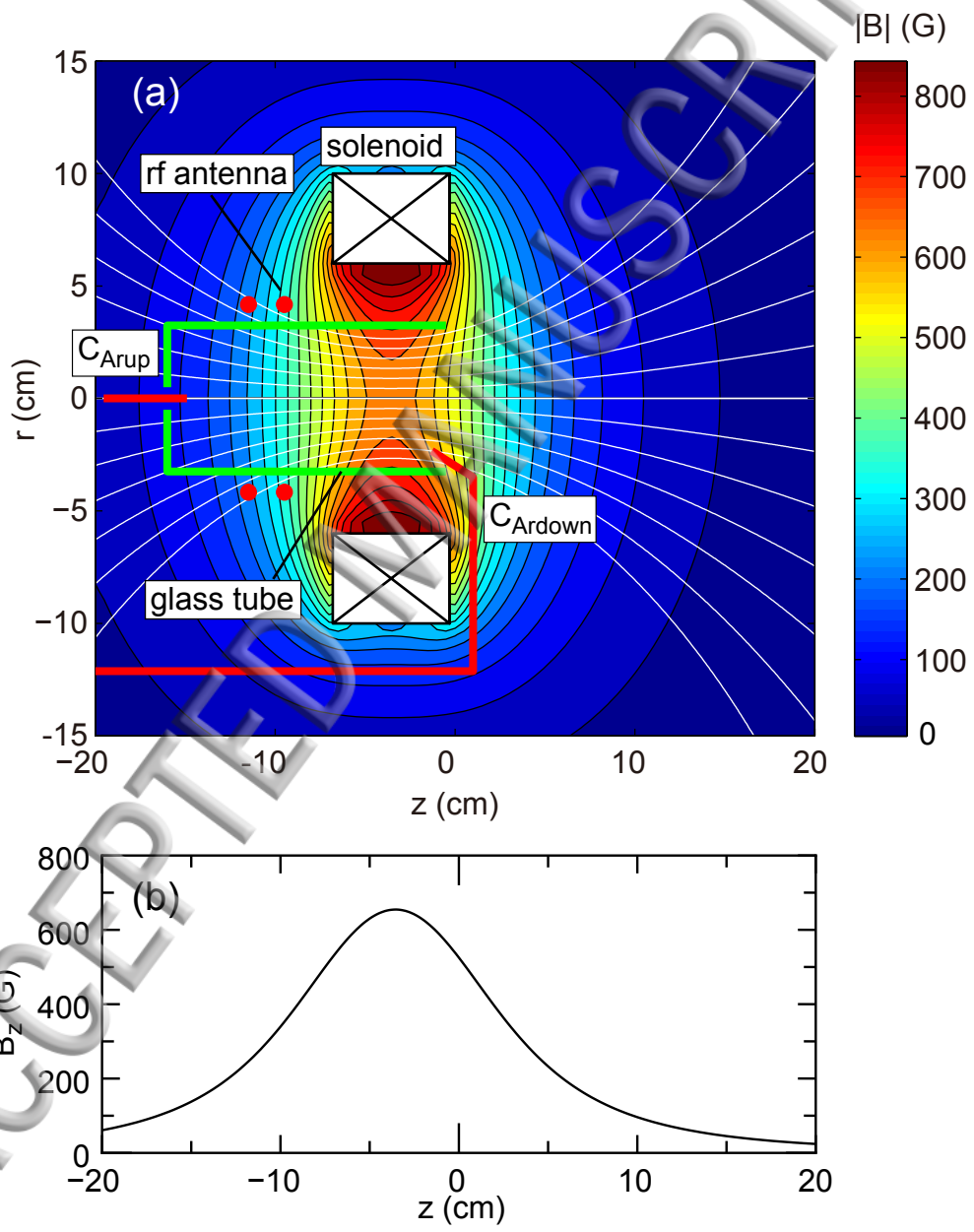

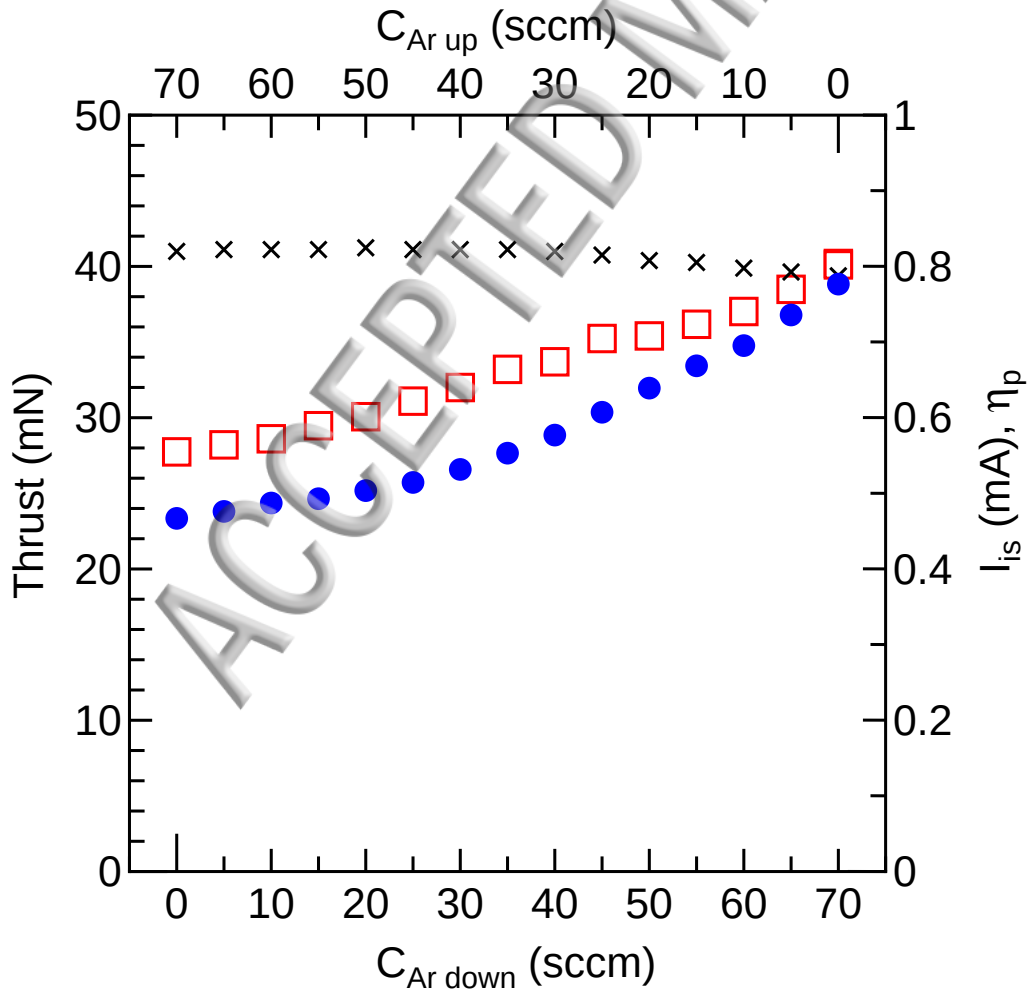
C_Ar up (sccm)
70 60 50 40 30 20 10 0
Thrust (mN)
50 40 30 20 10 0
I_is (mA), η_p
1 0.8 0.6 0.4 0.2 0
0 10 20 30 40 50 60 70
C_Ar down (sccm)

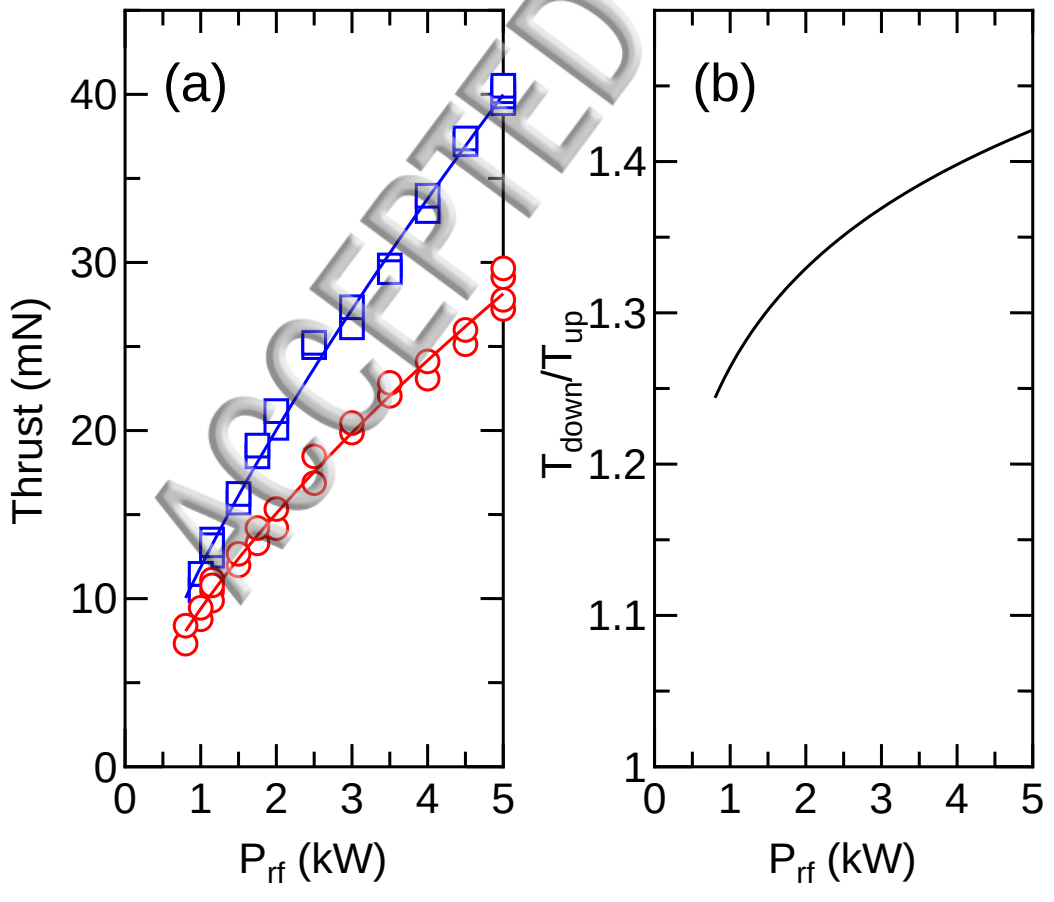
(a)
(b)
Thrust (mN)
T_{down}/T_{up}
P_{rf} (kW)
P_{rf} (kW)
0
10
20
30
40
1
1.1
1.2
1.3
1.4
0
1
2
3
4
5
ACCEPTED

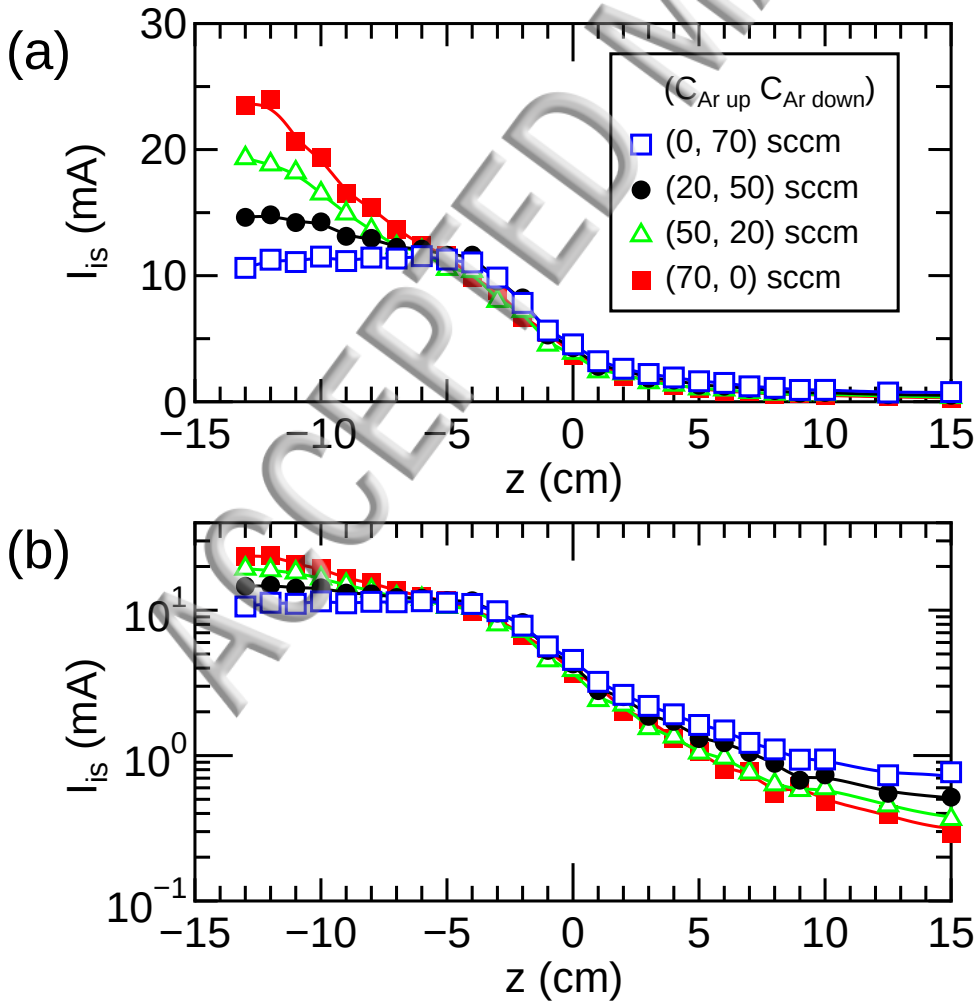
(a)
30
20
10
0
I_{is} (mA)
−15
−10
−5
0
5
10
15
z (cm)
($C_{Ar\ up}$ $C_{Ar\ down}$)
(0, 70) sccm
(20, 50) sccm
(50, 20) sccm
(70, 0) sccm
(b)
10^{1}
10^{0}
10^{-1}
I_{is} (mA)
−15
−10
−5
0
5
10
15
z (cm)